Monthly Notices
of the
ROYAL ASTRONOMICAL SOCIETY

MNRAS **483,** 654–663 (2019)
Advance Access publication 2018 November 27

doi:10.1093/mnras/sty3198

Towards converged electron-impact excitation calculations of low-lying transitions in Fe II

R. T. Smyth,[1]★ C. A. Ramsbottom,[1] F. P. Keenan,[2] G. J. Ferland[3] and C. P. Ballance[1]

[1]*Centre for Theoretical Atomic, Molecular and Optical Physics, School of Mathematics and Physics, Queen's University Belfast, Belfast BT7 1NN, Northern Ireland, UK*
[2]*Astrophysics Research Centre, School of Mathematics and Physics, Queen's University Belfast, Belfast BT7 1NN, Northern Ireland, UK*
[3]*Department of Physics and Astronomy, University of Kentucky, Lexington, KY 40506, USA*

Accepted 2018 November 15. Received 2018 November 15; in original form 2018 July 14

ABSTRACT

Absorption and emission lines of the iron-peak species Fe II are prominent in the infrared, optical, and ultraviolet spectra of a myriad of astrophysical sources, requiring extensive and highly reliable sets of atomic structure and collisional data for an accurate quantitative analysis. However, comparisons among existing calculations reveal large discrepancies in the effective collision strengths, often up to factors of three, highlighting the need for further steps towards new converged calculations. Here we report a new 20 configuration, 6069 level atomic structure model, calculated using the multiconfigurational Dirac–Fock method. Collision strengths and effective collision strengths are presented, for a wide range of temperatures of astrophysical relevance, from substantial 262 level and 716 level Dirac R-matrix calculations, plus a 716 level Breit–Pauli R-matrix calculation. Convergence of the scattering calculations is discussed, and results are critically compared with existing data in the literature, providing us with error estimates for our data. As a consequence, we assign an uncertainty of ±15 per cent to relevant forbidden and allowed transitions encompassed within a 50 level subset of the 716 level Dirac R-matrix data set. To illustrate the implications of our new data sets for the analysis of astronomical observations of Fe II, they are incorporated into the CLOUDY modelling code, sample Fe II spectra are generated and compared.

Key words: atomic data – atomic processes – scattering.

1 INTRODUCTION

Absorption and emission lines of the iron-peak species Fe II are widely detected in the spectra of a myriad of astrophysical sources, including active galactic nuclei (AGN), gaseous nebulae, supernovae remnants, and the interstellar medium. In particular, observations of the UV spectra of the symbiotic star AG Pegasi have led Eriksson, Johansson & Wahlgren (2006) to attribute 346 out of more than 600 observed lines to Fe II emission. More recent work by Carpenter et al. (2014) has shown that the far-UV spectrum of the K4 Ib-II supergiant λ Vel contains strong fluorescent Fe II emission features. The accurate quantitative analysis of such spectra depends upon high quality radiative and collisional data for Fe II. However, its complex open-d shell atomic structure renders the theoretical modelling a formidable task, requiring detailed configuration interaction expansions and large-scale scattering calculations. To this end, a variety of calculations have been undertaken in an attempt to produce high quality atomic data for astrophysical modelling.

Early calculations of Nussbaumer & Storey (1980) employed the close-coupling approximation with a two configuration basis, and presented collision strengths amongst the lowest four terms of Fe II. Additional work by Nussbaumer, Pettini & Storey (1981) provided collision strengths for dipole transitions between levels of the ground term and levels of the first three odd terms, using a distorted wave approximation. However, both calculations were limited in terms of the number of energy points considered (up to a maximum of three), thus omitting the effects of resonances. Later work of Baluja, Hibbert & Mohan (1986) employed the R-matrix method, but with only the first four terms of Fe II included in the close-coupling expansion. The resulting collision strengths displayed up to a factor of two discrepancy with previous results. A further R-matrix calculation by Berrington et al. (1988), incorporating spin-orbit effects, was then carried out with the lowest 16 fine-structure levels of Fe II (arising from the same four terms considered by Baluja et al. 1986) included in the close-coupling expansion. Their results disagreed with previous calculations and also highlighted inconsistencies in the calculations of Baluja et al. (1986) due to an imbalance between the descriptions of the N electron target expansion and the bound $(N+1)$ electron system. Keenan

★ E-mail: rsmyth41@qub.ac.uk, c.ramsbottom@qub.ac.uk

et al. (1988) extended the work of Berrington et al. (1988) to lower temperatures, providing effective collision strengths and the relative populations of fine-structure levels in the ground term relevant to interstellar medium studies. Comparisons with the work of Nussbaumer & Storey (1980) revealed discrepancies of up to a factor of two.

More extensive calculations by Pradhan & Berrington (1993) employed the non-relativistic R-matrix method with all 38 quartet and sextet terms from the $3d^6 4s$, $3d^7$, $3d^6 4p$ configurations, plus the Breit–Pauli R-matrix method with all 41 levels from the first 10 quartet and sextet terms of the $3d^6 4s$, $3d^7$, $3d^6 4p$ configurations. Zhang & Pradhan (1995) extended this Breit–Pauli R-matrix calculation to include all 142 levels arising from the 38 quartet and sextet terms. However, comparisons with previous results revealed large differences, mainly due to the increased size and sophistication of their calculations. Complementing the work of Zhang & Pradhan (1995) are two additional R-matrix calculations by Bautista & Pradhan (1996), which includes levels from the first 18 terms of Fe II, and Bautista & Pradhan (1998), that considers levels from the first 23 terms of Fe II. For the former it was noted that there were differences from previous work ranging from approximately 30 per cent up to factors of two, with weaker transitions in particular displaying large discrepancies.

Up to this point it was evident that no convergence of results for Fe II had been achieved. In light of this, the investigation of Ramsbottom et al. (2002) was undertaken to assess the accuracy of these existing calculations. This expanded on the work of Pradhan & Berrington (1993), using a finer energy mesh to better represent the low-energy resonance structures, and reporting on the importance of including all $(N + 1)$ configurations in the collision wavefunction. More sophisticated calculations by Ramsbottom et al. (2004) included all 113 terms in the close-coupling expansion arising from the $3d^6 4s$, $3d^7$, $3d^6 4p$, $3d^5 4s^2$, and $3d^5 4s4p$ configurations. Their work also presented an extensive set of 12 LS-coupled target models carefully exploring configuration interaction (CI) effects in for electron collisions with Fe II. Based on their analysis of the target models and collision strengths they note that their 26 configuration target model provides accurate low-energy LS-coupled collision strengths. This 26 configuration target model was then incorporated into investigations by Ramsbottom et al. (2005) to calculate collision strengths and effective collision strengths for the sextet to quartet forbidden transitions amongst the 113 terms of the $3d^6 4s$, $3d^7$, $3d^6 4p$, $3d^5 4s^2$, and $3d^5 4s4p$ basis configurations. While Ramsbottom et al. (2004) has discussed the importance of CI effects on the accuracy and degree of convergence of the collision strengths, the calculations of Fernández-Menchero, Del Zanna & Badnell (2015) for Be-like Al have further demonstrated that progressive convergence of calculations is achieved by increasing the size of the CI and close-coupling expansions.

Further work by Ramsbottom et al. (2007) presented extensive Breit–Pauli R-matrix calculations, including all 262 fine-structure levels from the 100 doublet, quartet and sextet LS terms of the $3d^6 4s$, $3d^7$, and $3d^6 4p$ configurations. Their paper focused on results for the lowest lying forbidden transitions and highlighted the lack of agreement with all previous level resolved calculations. The same 262 level model was also used by Ramsbottom (2009), this time concentrating on the dipole transitions. Work of Bautista et al. (2015) then presented a series of collision calculations making use of the R-matrix plus intermediate coupling frame transformation method, the Breit–Pauli R-matrix method and the Dirac R-matrix method. These calculations employed CI expansions including between 7 and 16 configurations and included 52 levels of the $3d^6 4s$, $3d^7$, $3d^5 4s^2$ configurations in the close-coupling expansions. Again, their effective collision strengths show large differences when compared to previous calculations. Recent work of Tayal & Zatsarinny (2018) employed the B-spline Breit–Pauli R-matrix method, including 340 fine structure levels of the $3d^6 4s$, $3d^7$, $3d^6 4p$, $3d^5 4s^2$, and $3d^5 4s4p$ configurations, along with semi-empirical fitting procedures to modify aspects of the target structure. Their calculations display reasonable agreement with few previous calculations but it is evident that some outliers still remain.

Despite this diverse range of calculations little agreement has been reached. This is particularly evident for the lowest lying forbidden transitions, the importance of which has been illustrated in the work of Smith & Hartigan (2006). They show that the near-IR spectrum of the nebula of P Cygni is dominated by emission lines originating from transitions amongst fine-structure levels of the lowest three terms of Fe II. For the $3d^6(^5D)4s\ ^6D_{9/2} - 3d^6(^5D)4s\ ^6D_{7/2}$ forbidden transition in particular, existing calculations display discrepancies of up to factors of three in the effective collision strengths. A further issue lies in the fact that existing work is limited with regards to the range of target levels included in the scattering calculations. For example, observations of the narrow-line quasar PHL 1811 Leighly et al. (2007) indicate that the near-UV region of its spectrum is dominated by strong Fe II lines, with emission from highly excited levels of Fe II up to 14 eV, an energy not explicitly reached by target levels included in existing calculations. Therefore, it is imperative that Fe II models are extended to include these highly excited target levels, to allow more detailed and reliable modelling of such objects.

The purpose of our paper is twofold. First, we address the disagreement among existing theoretical predictions for the low-lying forbidden and dipole transitions. Second, we extend existing scattering models to produce extensive sets of high quality atomic data for use in future astrophysical applications, such as a quantitative analysis of the spectra of PHL 1811. In Section 2 we present the current Fe II target models and discuss a 262 level Dirac R-matrix calculation, plus two substantial 716 level Breit–Pauli and Dirac R-matrix calculations. The latter two calculations, to our knowledge, are the largest investigations into the electron-impact excitation of Fe II to date, resulting in over 250 000 individual transitions. We provide collision strengths and effective collision strengths for a select few forbidden and allowed transitions, compare results with all existing available data in the literature, and discuss the convergence of our calculations. Finally, in Section 3 we briefly discuss the implications of our new Fe II data sets for the spectral modelling of astrophysical sources.

2 ELECTRON-IMPACT EXCITATION

2.1 Breit–Pauli R-matrix calculation

We first note that details of the underlying theory of the present R-matrix scattering calculations are well documented (see Burke 2011) and will therefore be omitted here. For the present Breit–Pauli R-matrix calculation, which is an extension of the work presented by Ramsbottom et al. (2007) and Ramsbottom (2009), we adopt the six configuration ($3d^6 4s$, $3d^7$, $3d^6 4p$, $3d^6 \overline{4d}$, $3d^5 4s^2$, $3d^5 4s4p$) Fe II target model 'A1' as presented in Ramsbottom et al. (2004). In this model the 1s, 2s, 2p, 3s, 3p, and 3d orbitals are taken from Clementi & Roetti (1974), while the 4s and 4p orbitals and $\overline{4d}$ pseudo-orbital were determined using the CIV3 atomic structure program of Hibbert (1975). A sample of target energies is given in

Table 1. Fine-structure target energies for the first 15 even parity and first 15 odd parity levels of Fe II, in Rydbergs (relative to the ground state), from the present 262 and 716 level DARC and 716 level Breit–Pauli calculations compared to existing models where available, and compared to experimental energies given in the NIST data base. R07 are the results of Ramsbottom et al. (2007); P93 are from Pradhan & Berrington (1993); and B88 from Berrington et al. (1988). Errors for the current DARC and Breit–Pauli target model energies are given in columns 5 and 7, respectively.

No.	Level	NIST	DARC	Error (per cent)	Breit–Pauli	Error (per cent)	R07	P93	B88
1	$3d^6(^5D)4s\ ^6D_{9/2}$	0.00000	0.00000	0.0	0.00000	0.0	0.00000	0.00000	0.00000
2	$3d^6(^5D)4s\ ^6D_{7/2}$	0.00351	0.00323	8.0	0.00398	13.4	0.00398	0.00315	0.00324
3	$3d^6(^5D)4s\ ^6D_{5/2}$	0.00608	0.00562	7.6	0.00695	14.3	0.00695	0.00558	0.00560
4	$3d^6(^5D)4s\ ^6D_{3/2}$	0.00786	0.00728	7.4	0.00903	14.8	0.00903	0.00731	0.00725
5	$3d^6(^5D)4s\ ^6D_{1/2}$	0.00890	0.00825	7.3	0.01025	15.1	0.01025	0.00834	0.00822
6	$3d^7\ ^4F_{9/2}$	0.01706	0.01757	3.0	0.02786	63.3	0.02898	0.06404	0.05030
7	$3d^7\ ^4F_{7/2}$	0.02215	0.02197	0.8	0.03315	49.7	0.03428	0.06860	0.05540
8	$3d^7\ ^4F_{5/2}$	0.02586	0.02523	2.4	0.03707	43.3	0.03820	0.07200	0.05930
9	$3d^7\ ^4F_{3/2}$	0.02841	0.02748	3.3	0.03977	40.0	0.04091	0.07450	0.06210
10	$3d^6(^5D)4s\ ^4D_{7/2}$	0.07249	0.10600	46.2	0.07232	0.2	0.07233	0.09110	0.09110
11	$3d^6(^5D)4s\ ^4D_{5/2}$	0.07647	0.10983	43.6	0.07694	0.6	0.07696	0.09480	0.09470
12	$3d^6(^5D)4s\ ^4D_{3/2}$	0.07910	0.11222	41.9	0.08005	1.2	0.08007	0.09730	0.09730
13	$3d^6(^5D)4s\ ^4D_{1/2}$	0.08062	0.11363	41.0	0.08186	1.5	0.08187	0.09890	0.09890
14	$3d^7\ ^4P_{5/2}$	0.12279	0.10860	11.6	0.14864	21.1	0.15040	0.19900	0.17180
15	$3d^7\ ^4P_{3/2}$	0.12460	0.11062	11.2	0.15096	21.2	0.15270	0.19900	0.17480
16	$3d^6(^5D)4p\ ^6D^o_{9/2}$	0.35046	0.35388	1.0	0.31984	8.7	0.32084	0.33300	–
17	$3d^6(^5D)4p\ ^6D^o_{7/2}$	0.35230	0.35563	0.9	0.32231	8.5	0.32334	0.33500	–
18	$3d^6(^5D)4p\ ^6D^o_{5/2}$	0.35411	0.35723	0.9	0.32455	8.3	0.32557	0.33700	–
19	$3d^6(^5D)4p\ ^6D^o_{3/2}$	0.35551	0.35855	0.9	0.32625	8.2	0.32725	0.33900	–
20	$3d^6(^5D)4p\ ^6D^o_{1/2}$	0.35639	0.35934	0.8	0.32730	8.2	0.32830	0.34000	–
21	$3d^6(^5D)4p\ ^6F^o_{11/2}$	0.38244	0.39779	4.0	0.35625	6.8	0.35724	0.36600	–
22	$3d^6(^5D)4p\ ^6F^o_{9/2}$	0.38378	0.39918	4.0	0.35926	6.6	0.35929	0.36800	–
23	$3d^6(^5D)4p\ ^6F^o_{7/2}$	0.38489	0.40016	4.0	0.35988	6.5	0.36092	0.37000	–
24	$3d^6(^5D)4p\ ^6F^o_{5/2}$	0.38578	0.40105	4.0	0.36111	6.4	0.36214	0.37100	–
25	$3d^6(^5D)4p\ ^6F^o_{3/2}$	0.38640	0.40160	3.9	0.36197	6.3	0.36298	0.37200	–
26	$3d^6(^5D)4p\ ^6F^o_{1/2}$	0.38674	0.40192	3.9	0.36247	6.3	0.36348	0.37200	–
27	$3d^6(^5D)4p\ ^6P^o_{7/2}$	0.38873	0.40085	3.1	0.36793	5.4	0.37600	0.38400	–
28	$3d^6(^5D)4p\ ^6P^o_{5/2}$	0.39402	0.40587	3.0	0.37358	5.2	0.38175	0.38800	–
29	$3d^6(^5D)4p\ ^6P^o_{3/2}$	0.39750	0.40929	3.0	0.37735	5.1	0.38559	0.39100	–
30	$3d^6(^5D)4p\ ^4F^o_{9/2}$	0.40308	0.43800	8.7	0.38910	3.5	0.38559	0.40300	–

Table 1, and compared to the previous calculations of Ramsbottom et al. (2007), Pradhan & Berrington (1993), and Berrington et al. (1988). Overall, when compared with experimental values given in the NIST data base (2018), our 716 target levels have an average error of approximately 10.3 per cent. The even parity levels have an average error of 21.6 per cent, ranging from 0.0002 per cent to 63.3 per cent, while the odd parity levels have an average error of 8.1 per cent, ranging from 0.3 per cent up to 16.3 per cent. We note that the $3d^7\ ^4F_J$ ($J = \frac{9}{2}, \frac{7}{2}, \frac{5}{2}, \frac{3}{2}$) levels (numbered 6–9 in Table 1) are the largest source of errors.

The scattering calculation included all 716 fine-structure levels arising from the 261 LS terms of the $3d^64s$, $3d^7$, $3d^64p$, $3d^54s^2$, and $3d^54s4p$ configurations. Although $3d^6\overline{4d}$ was included for CI, terms of this configuration were omitted from the close-coupling expansion. The $(N + 1)$ bound configurations included in the calculation were of the form $3d^7\{4s, 4p, 4d\}$; $3d^6\{4s^2, 4p^2, 4d^2, 4s4p; 4s4d, 4p4d\}$; $3d^5\{4s^24p, 4s^24d, 4s4p^2, 4s4p4d\}$; and $3d^8$. We considered partial waves with total angular momenta $L \leq 37$ and $1 \leq (2S + 1) \leq 9$ for both even and odd parities, allowing us to span all $J\pi$ partial waves from $2J = 0$ to $2J = 60$. 15 continuum basis orbitals were employed for partial waves $2J = 0$ up to $2J = 26$, which then was reduced to 11 for the remaining higher partial waves $2J = 28$ up to $2J = 60$. The size of the R-matrix boundary was set at 15 atomic units, a maximum of 5075 coupled channels were obtained, and Hamiltonian matrices of sizes up to 61051 × 61051 diagonalized. All 716 target energies were shifted to the experimental values given in the NIST data base, to ensure that target thresholds and wavelengths agreed with observations. This was achieved by changing the individual diagonal elements of the target Hamiltonian prior to its diagonalization.

A very fine mesh was used to delineate the complex resonance structures, using 22 300 energy points with a spacing of 10^{-4} Ryd for partial waves $2J = 0$ up to $2J = 26$. For the remaining higher partial waves, a coarse mesh of 300 points with a spacing of approximately 10^{-2} Ryd was used. Finally, to estimate contributions to the dipole transitions from partial waves $2J > 60$, a 'top-up' procedure described by Burgess (1974) was employed.

2.2 Dirac R-matrix calculations

Our DARC calculations were undertaken to corroborate results obtained from the 716 level Breit–Pauli R-matrix one discussed in Section 2.1, using independent methods for both the atomic structure and the electron-impact excitation. The target model for the former was determined using the multiconfigurational Dirac–Fock (MCDF) method implemented by GRASP^0 (Dyall et al. 1989; Parpia & Grant 1991). We note that initial convergence problems with the 3d and 4d orbitals were encountered. However, this issue

was alleviated by considering an initial set of fully converged orbitals from the neighbouring Co III ion, obtained from a calculation which included highly occupied 3d and 4d configurations. The resulting orbitals were subsequently used as a starting point for the Dirac–Fock iterative process in the Fe II calculation.

Our initial MCDF calculation included the $3d^7$; $3d^6\{4s, 4p, 4d, 5s, 5p\}$; $3d^5\{4s^2, 4p^2, 4d^2, 4s4p, 4s4d, 5s^2, 5p^2\}$; $3p^4\{3d^9, 4d^9\}$; $3p^63d^14d^6$; $3p^63d^24d^5$; and $3p^63d^34d^4$ configurations, and all orbitals were variationally determined by employing the extended average level (EAL) method, once for Co III and then once for Fe II as described above. One final EAL calculation with the $3d^54s4d$; $3p^44d^9$; $3p^63d^14d^6$; $3p^63d^24d^5$; and $3p^63d^34d^4$ configurations removed, the $3p^53d^7\{4s, 4p, 5s\}$; $3p^53d^6\{4s^2, 4s5s\}$; $3p^43d^84s$; and $3p^43d^74s^2$ configurations included, and also holding the 3d and 4d orbitals fixed, yielded our final Fe II atomic structure. The full 20 configuration, 6069 level model was taken through to the Dirac R-matrix calculations. However, we chose to retain only the first 262 and 716 levels of our target structure in the close-coupling expansions of the collision wavefunctions. A selection of fine-structure target energies are presented in Table 1. When compared with the NIST values our 262 level target model has an overall average error of 9.3 per cent. Even parity levels have an average error of 10.9 per cent, ranging from 0.8 per cent to 21.8 per cent with four individual outliers ranging from 41.0 per cent to 46.2 per cent due to the $3d^6(^5D)4s\ ^4D_J$ ($J = \frac{7}{2}, \frac{5}{2}, \frac{3}{2}, \frac{1}{2}$) levels (numbered 10–13 in Table 1). The odd parity levels are well represented, with an average error of 7.9 per cent, ranging from 0.8 per cent to 18.7 per cent. Similarly, our 716 level target model has an overall average error of 11.3 per cent, with averages of 13.8 per cent and 10.2 per cent for the even parity and odd parity levels, respectively. Main sources of error are due to a small number of some highly excited levels in the target description.

We note that our current 20 configuration GRASP^0 target model considerably improves upon the GRASP^0 model of Bautista et al. (2015) which bears an average error of 20 per cent, this compared to the average errors of 9.3 per cent and 11.3 per cent for our 262 and 716 level models, respectively. In particular, we note that these existing GRASP^0 calculations fail to include a fully variationally determined 4d orbital, which is in contrast to our present 20 configuration calculation. The implications of such an omission has been highlighted in Bautista et al. (2015), showing that without a properly calculated 4d orbital to account for the relaxation effects of the 3d orbital, poor agreement with observed spectra will be seen. Additionally, statistically averaging our fine-structure resolved atomic structure model reveals (when the first 16 terms are considered) an average error of 15 per cent. Comparing with the calculated term energies of Bautista et al. (2015) we see good agreement with the results of their 16 configuration 'NewTFDAc' model, showing only a 6 per cent overall difference with the present statistically averaged GRASP^0 results. Good agreement is also seen with the 26 configuration LS-coupled CIV3 model of Ramsbottom et al. (2004), exhibiting an overall difference of 9 per cent.

The 262 level scattering calculation included all $J\pi$ partial waves from $2J = 0$ up to $2J = 60$, with 15 continuum basis orbitals for each value of angular momentum, and we set the R-matrix boundary at 19.84 atomic units. This calculation resulted in Hamiltonian matrices of sizes up to $34\,895 \times 34\,895$ and up to 1850 coupled channels. A fine energy mesh was used to delineate the resonance structures, this time with 16 000 energy points and an energy spacing of 1.25×10^{-4} Ryd for all partial waves. For the 716 level calculation we included partial waves from $2J = 0$ up to $2J = 60$, this time with 13 continuum basis orbitals and another R-matrix boundary at 19.84 atomic units. This calculation resulted in up to 5252 coupled channels and Hamiltonian matrices of sizes up to $72\,694 \times 72\,694$. Another fine energy mesh of 16 000 energy points and an energy spacing of 1.25×10^{-4} Ryd was employed for $2J = 0$ up to $2J = 26$, and a much coarser mesh of 800 points with an energy spacing of 2.5×10^{-3} Ryd was used for the reminder. In both calculations, all energy levels were shifted to the experimental values given in the NIST data base, and 'top-up' procedures employed to estimate contributions from higher partial waves $2J > 60$.

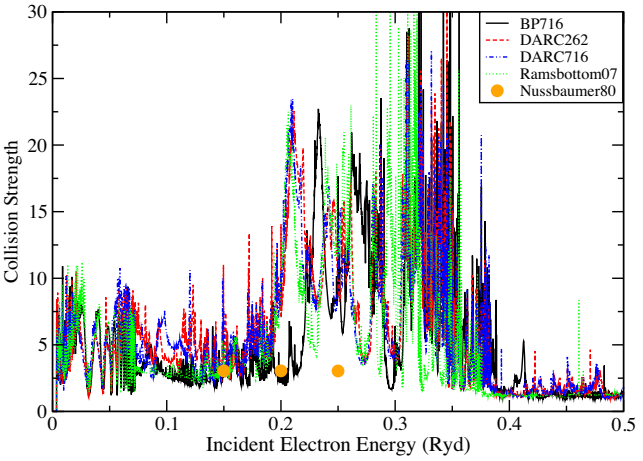

Figure 1. Collision strengths for the $3d^6(^5D)4s\ ^6D_{9/2} - 3d^6(^5D)4s\ ^6D_{7/2}$ forbidden transition (labelled 1–2 from Table 1). The solid black line is the result from BP716, the dashed red line is from DARC262, the blue dash–dot line from DARC716, the dotted green line from Ramsbottom et al. (2007), and orange circles from Nussbaumer & Storey (1980).

2.3 Results and discussion

To illustrate our results, we present the collision strengths Ω_{ij}, for transitions from initial levels i to final levels j, and the corresponding effective collision strengths Υ_{ij}, defined as

$$\Upsilon_{ij}(T_e) = \int_0^\infty \Omega_{ij} \exp\left(-\frac{\epsilon_j}{kT_e}\right) \mathrm{d}\left(\frac{\epsilon_j}{kT_e}\right), \quad (1)$$

which is of more practical use in plasma modelling applications. In equation (1), ε_j is the scattered electron kinetic energy, T_e the electron temperature in Kelvin, and k is Boltzmann's constant. For brevity, we refer to the 716 level Breit–Pauli R-matrix calculation as BP716, and the 262 level and 716 level DARC calculations as DARC262 and DARC716, respectively. The 262 level Breit–Pauli calculations of Ramsbottom et al. (2007) and Ramsbottom (2009) are termed R07 and R09, respectively.

In Fig. 1 we present the collision strengths for the low-lying $3d^6(^5D)4s\ ^6D_{9/2} - 3d^6(^5D)4s\ ^6D_{7/2}$ forbidden transition (labelled 1–2 from Table 1) from the current BP716, DARC262, and DARC716 calculations, and compare with the results of R07 and Nussbaumer & Storey (1980). We see that there is generally good agreement between the present data and those of R07. However, the DARC262 and DARC716 results lie slightly higher than both BP716 and R07 in the 0.075–0.15 Ryd energy range. There are also some discrepancies in terms of the broad resonance positions in the 0.20–0.30 Ryd interval. It is interesting to note that better agreement is found between both the 262 and 716 level DARC calculations and R07 up to approximately 0.27 Ryd, beyond which the discrepancies between DARC262, DARC716, and BP716 are the smallest.

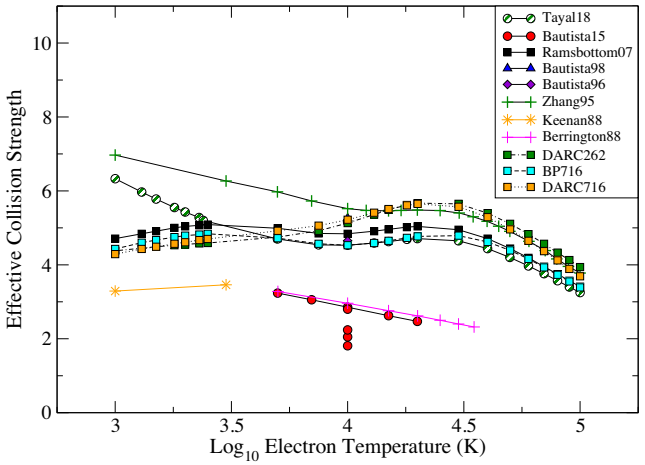

Figure 2. Effective collision strengths for the $3d^6(^5D)4s\ ^6D_{9/2} - 3d^6(^5D)4s\ ^6D_{7/2}$ transition (labelled 1–2 from Table 1). Cyan squares with the dashed line are the current BP716 results, green squares with the dash–dot line are from DARC262, and orange squares with the dotted line are from DARC716. Patterned circles are results of Tayal & Zatsarinny (2018); solid red circles are from various models of Bautista et al. (2015); black squares with the solid line are from Ramsbottom et al. (2007); blue triangles from Bautista & Pradhan (1998); purple diamonds from Bautista & Pradhan (1996); green crosses from Zhang & Pradhan (1995); orange stars from Keenan et al. (1988); and pink plus signs from Berrington et al. (1988).

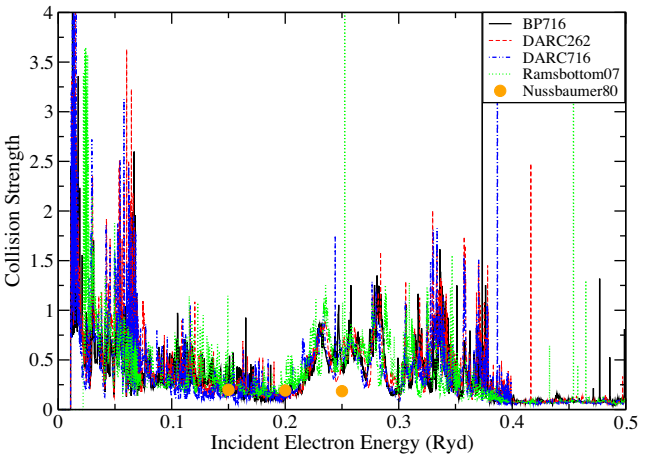

Figure 3. Collision strengths for the $3d^6(^5D)4s\ ^6D_{5/2} - 3d^7\ ^4F_{9/2}$ forbidden transition (labelled 3–6 from Table 1). The solid black line is the result from BP716, the dashed red line is from DARC262, the blue dash–dot line is from DARC716, the dotted green line from Ramsbottom et al. (2007), and orange circles from Nussbaumer & Storey (1980).

The corresponding effective collision strengths are presented in Fig. 2 for a sample $10^3 - 10^5$ K temperature range, and compared to all available results in the literature. It is clear that the present DARC262, DARC716, and BP716 data and those of R07 exhibit very good agreement in both shape and magnitude. Across the entire energy range there is an average difference of 2 per cent between DARC262 and DARC716. Similarly, we have an overall average difference of 8 per cent between DARC716 and BP716. At a temperature of 10^4 K (approximately the temperature of maximum abundance of Fe II in ionization equilibrium) good agreement is found with the data of Bautista & Pradhan (1996), Bautista & Pradhan (1998), and with the single reported result of a six configuration DARC calculation by Bautista et al. (2015). Very good agreement is seen between BP716 and the results of Tayal & Zatsarinny (2018) in both shape and magnitude at intermediate to high temperatures. However, at lower temperatures there is a greater disparity. Additionally, very good agreement is seen between DARC716 and the results of Zhang & Pradhan (1995) at temperatures above 10^4 K. Again, at lower temperatures, the results of Zhang & Pradhan (1995) do not show the same level of agreement. Furthermore, it is evident that there is no agreement with the results of Berrington et al. (1988) or Keenan et al. (1988), nor with remaining results of Bautista et al. (2015). These results in particular stem from calculations which adopt target structures consisting of only even parity configurations. The investigations of Zhang & Pradhan (1995) and Ramsbottom et al. (2005) show that the low metastable levels are strongly coupled to excited odd parity states, giving rise to additional resonance features in the collision strengths. The omission of odd parity target states in the scattering calculations will ultimately result in erroneous effective collision strengths as a direct result of these missing resonances. Since the six configuration DARC calculation of Bautista et al. (2015) does in fact include odd parity target states in the close-coupling expansion, the effective collision strengths are larger, agreeing better with the present calculations. In contrast, the remaining calculations of Bautista et al. (2015) do not include odd parity states and the effective collision strengths are therefore lower.

The work of Bautista et al. (2015) also attributes significant variations between results to the shifting of target energies. However, we note that the target thresholds in the work of R07 were not shifted to experimental values, while the present BP716 target thresholds were indeed shifted to coincide with experimental values. Referring to Table 1 we see that the target structures employed in these two calculations are extremely similar and it is evident from Fig. 2 that there are no substantial differences between the effective collision strengths of BP716 and R07. We see that only a small difference of 4 per cent exists overall. By extension, since the target representations used in DARC262 and DARC716 are of higher accuracy than those used in R07 and BP716, we are confident that shifting those target thresholds will also not lead to any substantial changes in the effective collision strengths.

Collision strengths for the $3d^6(^5D)4s\ ^6D_{5/2} - 3d^7\ ^4F_{9/2}$ forbidden transition from the ground state complex (labelled 3–6 from Table 1) are presented in Fig. 3. Overall we see very good agreement among the present BP716, DARC262, and DARC716 results. However, across portions of the shown energy range the dense resonances structures from BP716 are smaller than those from both DARC262 and DARC716. There are also little discrepancies with two out of the three collision strengths of Nussbaumer & Storey (1980), while BP716, DARC262, and DARC716 show very good overall agreement with R07. However, since the target levels of R07 were not shifted to experimental values, the resonances near the excitation threshold lie slightly further up the energy range. Furthermore, given the high level of agreement between the 262 and 716 level calculations, as seen from Figs 2 and 3, we can deduce that our close-coupling expansion has certainly converged for low-lying forbidden transitions. It is clear that we have also reached convergence in terms of the employed energy mesh sizes, discussed in Sections 2.1 and 2.2, with no discernible differences in resolution between a mesh with 16 000 energy points and one with 22 300.

The corresponding effective collision strengths are presented in Fig. 4. There is very good agreement between the current DARC262 and DARC716 values and those of R07. However, at lower temperatures BP716 is, at most, a factor of 1.3 times smaller than these

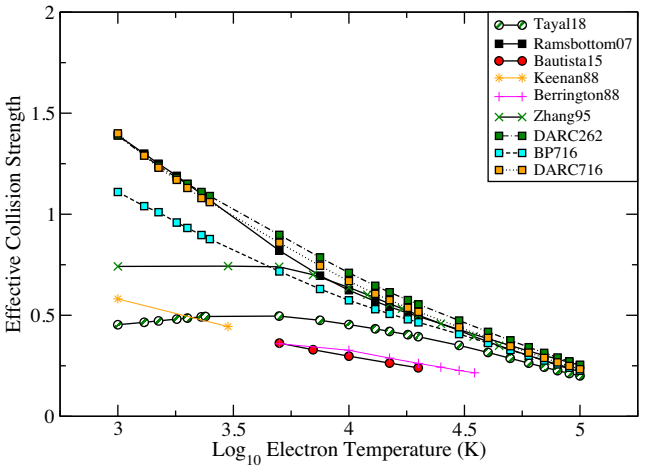

Figure 4. Effective collision strengths for the $3d^6(^5D)4s\ ^6D_{5/2} - 3d^7\ ^4F_{9/2}$ transition (labelled 3–6 from Table 1). Cyan squares with the dashed line are the current BP716 results, green squares with the dash–dot line are from DARC262 and orange squares with the dotted line are from DARC716. Patterned circles are results of Tayal & Zatsarinny (2018); solid red circles are from various models of Bautista et al. (2015); black squares with the solid line are from Ramsbottom et al. (2007); green crosses are from Zhang & Pradhan (1995); orange stars are from Keenan et al. (1988); and pink plus signs are from Berrington et al. (1988).

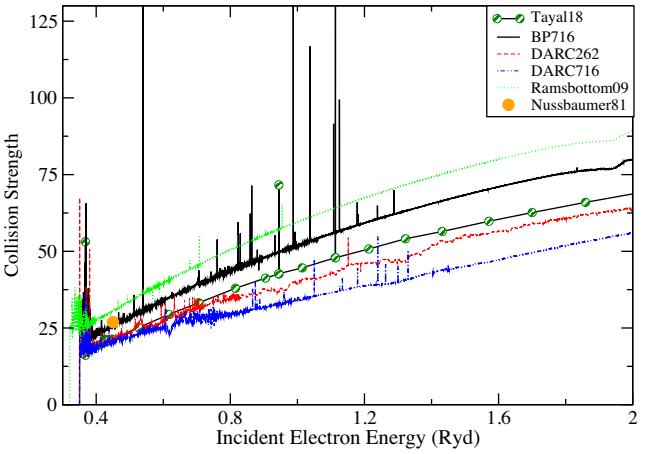

Figure 5. Collision strengths for the $3d^6(^5D)4s\ ^6D_{9/2} - 3d^6(^5D)4p\ ^6D^o_{9/2}$ dipole transition (labelled 1–16 from Table 1). The solid black line is the result from BP716, the dashed red line is from DARC262, the blue dash–dot line is from DARC716, patterned circles are from Tayal & Zatsarinny (2018), the dotted green line is from Ramsbottom (2009), and orange circles are from Nussbaumer et al. (1981).

three sets of effective collision strengths, with agreement becoming much better as the electron temperature increases. This discrepancy at the lower temperatures is most likely due to the differences in the heights of the dense resonance structures near the excitation threshold as mentioned previously. At the highest temperatures there is excellent agreement. Across the shown temperature range we have an average difference of 5 per cent between DARC262 and DARC716, and an average of 12 per cent between DARC716 and BP716. Similar to before, comparisons of BP716, DARC262, and DARC716 with the results of Zhang & Pradhan (1995) show that there is good agreement in terms of magnitude and shape from 5000 K onwards. At the lowest temperatures there is very little agreement with the results of Tayal & Zatsarinny (2018), owing to the sensitivity of the effective collision strengths on the complex resonance structures within the corresponding collision strengths. However, agreement in shape and magnitude improves as the temperature increases, with their results clearly converging to the same point as the present DARC262, DARC716, and BP716. Again, the results of Keenan et al. (1988), Berrington et al. (1988), and Bautista et al. (2015) are much too low. As discussed above, this may be due to the omission of odd parity target states in the close-coupling expansions.

In Fig. 5 we present the collision strengths for the first dipole transition $3d^6(^5D)4s\ ^6D_{9/2} - 3d^6(^5D)4p\ ^6D^o_{9/2}$ (1–16). We first note that subtle pseudo-resonances are present in the DARC262 collision strengths associated with the truncation of such a large target structure. However, it is evident that they are no longer present in DARC716. The collision strengths from the Breit–Pauli calculations (R09 and the current BP716) are higher than those from both present DARC calculations (DARC262 and DARC716). In Fig. 5 we also present the collision strength of Tayal & Zatsarinny (2018), which falls below BP716 and appears to lie above and agree well with DARC262, especially below 0.7 Ryd. However, an examination of the atomic structure calculations reveals the reason for the apparent disparities. The Breit–Pauli models yield a radiative transition rate of 3.28×10^8 s^{-1}. This compared to the rate of 2.75×10^8 s^{-1} presented by Tayal & Zatsarinny (2018), the DARC rate of 2.53×10^8 s^{-1}, and the experimental rate of 2.35×10^8 s^{-1} from the NIST data base. It is clear that the DARC value is closer to the experimental one, differing by only 7.4 per cent.

We also note a reduction in the magnitudes of the collision strengths when the size of the target descriptions are increased from 262 to 716 levels, which we attribute to configuration mixing. The present atomic structure calculations show that the upper $3d^6(^5D)4p\ ^6D^o_{9/2}$ level of this dipole transition is mixed with some highly excited levels of the $3d^64p$, $3d^54s4p$ and $3d^65p$ configurations, which are included in the 716 level targets but not the 262 level targets. In particular, we note that there is mixing with $3d^5(^4G)4s4p(^3P^o)\ ^6F^o_{9/2}$ at 0.7971 Ryd and $3d^5(^4D)4s4p(^3P^o)\ ^6D^o_{9/2}$ at 0.8571 Ryd, which have large radiative rates to the ground state of 3.47×10^8 s^{-1} and 6.61×10^8 s^{-1}, respectively. The inclusion of these levels in the target descriptions will ultimately result in a drop in the collision strength of the $3d^6(^5D)4s\ ^6D_{9/2} - 3d^6(^5D)4p\ ^6D^o_{9/2}$ transition to account for this additional mixing, highlighting the importance of including a larger number of highly excited levels in the close-coupling expansion to achieve convergence. We also note that the mixing of $3d^6(^5D)4p\ ^6D^o_{9/2}$ with even more highly excited levels beyond the current 716 level target description is relatively small. Therefore, we expect that including more than 716 levels in the calculations will not change the collision strength by any significant amount, indicating convergence of the close-coupling expansion.

Finally, in Fig. 6 the effective collision strengths for the $3d^6(^5D)4s\ ^6D_{9/2} - 3d^6(^5D)4p\ ^6D^o_{9/2}$ dipole transition are presented. Despite the reduction in the collision strengths as shown in Fig. 5, there is good agreement in shape and magnitude between DARC262 and DARC716, and also good agreement between BP716 and R09. The results of Zhang & Pradhan (1995) fall midway between the DARC and Breit–Pauli calculations at intermediate to higher temperatures but lies below them at the lowest temperatures. We also see very good agreement between our DARC262 model and the results of Tayal & Zatsarinny (2018) with an overall difference of only 5.3 per cent between them.

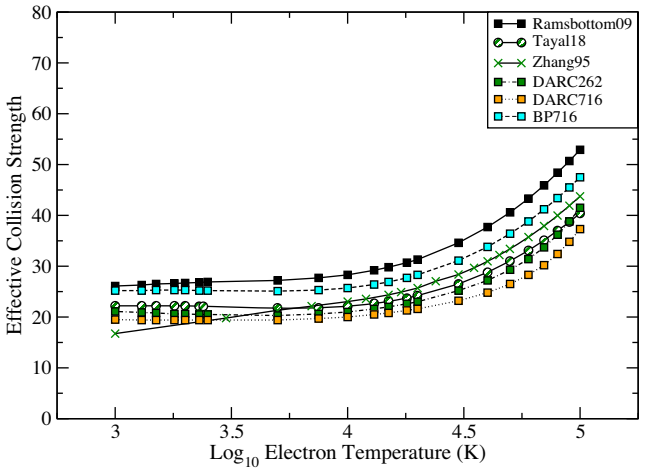

Figure 6. Effective collision strengths for the $3d^6(^5D)4s\ ^6D_{9/2} - 3d^6(^5D)4p\ ^6D^o_{9/2}$ transition (labelled 1–16 from Table 1). Cyan squares with the dashed line are the current BP716 results, green squares with the dash–dot line are the current DARC262 results, and orange squares with the dotted line are those from DARC716. Patterned circles are results of Tayal & Zatsarinny (2018); black squares with the solid line are from Ramsbottom (2009); green crosses from Zhang & Pradhan (1995).

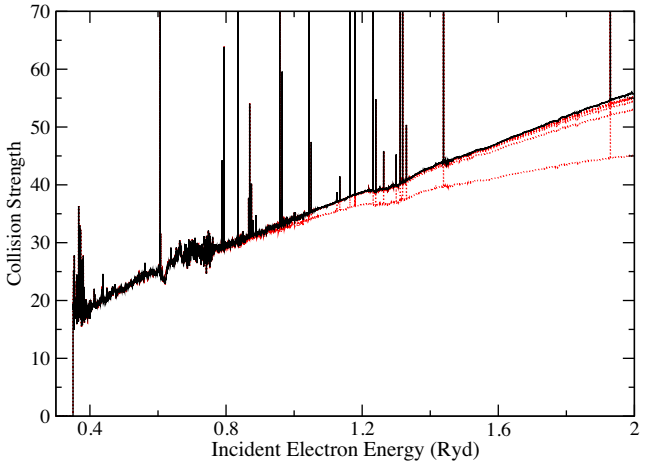

Figure 7. Plot showing a partial wave breakdown of the collision strengths for the $3d^6(^5D)4s\ ^6D_{9/2} - 3d^6(^5D)4p\ ^6D^o_{9/2}$ (labelled 1–16 from Table 1) dipole transition. We include (from bottom to top) all $J\pi$ partial waves up to $2J = 26$, 40, 48, 54, 58, 60 without top-up, and finally 60 with top-up.

Additionally, further convergence of our calculations can be demonstrated by considering the breakdown of the partial wave expansion. We clearly illustrate this using, as an example, the DARC716 collision strength for the $3d^6(^5D)4s\ ^6D_{9/2} - 3d^6(^5D)4p\ ^6D^o_{9/2}$ dipole transition. From Fig. 7 we see that the lowest $J\pi$ partial waves included in the calculation provide the greatest contributions to the collision strength. Including higher partial waves, $2J = 28$ up to $2J = 40$, gives up to a 17.7 per cent increase in the collision strength. Similarly, including $2J = 42$ up to $2J = 48$ we see up to a 2.7 per cent increase, while including $2J = 50$ up to $2J = 54$ leads up to a 1.7 per cent increase. The final few partial waves $2J = 56$ up to $2J = 60$ without 'top-up' gives a very small increase of 0.2 per cent, while 'top-up' estimations for all $2J > 60$ provides an increase of 1.1 per cent.

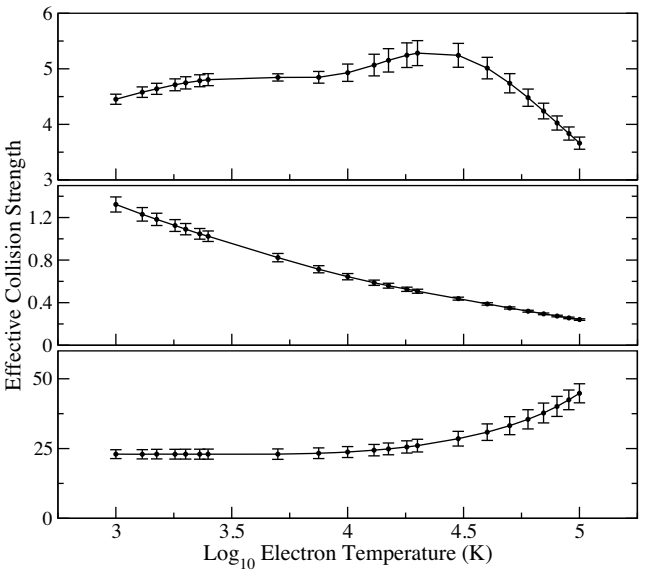

Figure 8. Plot showing the mean of the effective collision strengths with error bars provided at each temperature. Top panel, $3d^6(^5D)4s\ ^6D_{9/2} - 3d^6(^5D)4s\ ^6D_{7/2}$ (1–2) transition; middle, $3d^6(^5D)4s\ ^6D_{9/2} - 3d^7\ ^4F_{9/2}$ (3–6) transition; bottom, $3d^6(^5D)4s\ ^6D_{9/2} - 3d^6(^5D)4p\ ^6D^o_{9/2}$ (1–16) transition.

Given the more detailed nature of the 20 configuration GRASP^0 target structure that was taken through in full to the scattering calculations and its overall good agreement with experimental values, and since convergence of the scattering calculation has clearly been illustrated, we choose to make the 716 level DARC data set available to those requiring an extensive set of Fe II atomic data for modelling purposes.

2.4 Uncertainty estimates

We will now provide an analysis of the uncertainties associated with the present DARC716 data set. Despite their usefulness in astrophysical modelling, we note that there are very few uncertainty estimates for existing Fe II collisional data sets in the literature. However, we do note that the recent work of Bautista et al. (2015) provided a discussion of the uncertainties in their atomic rates by analysing the dispersion of data amongst their various models. Similarly, Tayal & Zatsarinny (2018) provided a discussion of the uncertainties in their 340 level data set by comparing their atomic data with the data sets of Bautista et al. (2015), R07, and Zhang & Pradhan (1995). For our discussion of uncertainties we will consider the deviations amongst the present three BP716, DARC262, and DARC716 calculations and also with the existing 262 level data sets of R07/R09. One point, evident from Section 2.3, is the good overall agreement in terms of shape and magnitude among BP716, DARC262, DARC716, and R07/R09. Therefore, it would not be unreasonable to make use of the mean of these effective collision strengths and assign a margin of error at each temperature point. To this end we use these four data sets to calculate the standard deviation from the mean σ_m at each individual temperature point, allowing us to assign an uncertainty of $\pm\sigma_m/\sqrt{4}$ to the mean effective collision strength.

In Fig. 8 we present the mean effective collision strengths and their associated uncertainties (shown as error bars) for transitions presented in the previous section. For the $3d^6(^5D)4s\ ^6D_{9/2} - 3d^6(^5D)4s\ ^6D_{7/2}$ (1–2) transition we have an overall average

Table 2. Table showing the uncertainty in the mean effective collision strengths of DARC262, DARC716, BP716, and R07/R09 calculations for the $3d^6(^5D)4s\ ^6D_{9/2} - 3d^6(^5D)4s\ ^6D_{7/2}$ (1–2) transition, $3d^6(^5D)4s\ ^6D_{5/2} - 3d^7\ ^4F_{9/2}$ (3–6) transition, and the $3d^6(^5D)4s\ ^6D_{9/2} - 3d^6(^5D)4p\ ^6D^o_{9/2}$ (1–16) transition.

	Uncertainty (per cent)		
$\log_{10}(T_e)$	Transition 1–2	Transition 3–6	Transition 1–16
3.000	2.03	5.36	6.87
3.114	2.07	5.15	7.24
3.176	2.14	4.87	7.46
3.255	2.27	4.93	7.64
3.301	2.32	4.86	7.71
3.362	2.24	4.81	7.79
3.398	2.25	4.83	7.86
3.699	1.35	4.72	8.16
3.875	2.17	4.70	8.17
4.000	3.17	4.54	8.26
4.114	3.85	4.23	8.36
4.176	4.08	4.09	8.47
4.255	4.23	3.83	8.59
4.301	4.26	3.70	8.71
4.477	4.14	3.19	9.22
4.602	3.96	2.92	9.61
4.699	3.85	2.82	9.73
4.778	3.75	2.73	9.70
4.845	3.77	2.76	9.42
4.903	3.68	2.80	8.94
4.954	3.67	2.92	8.31
5.000	3.61	3.07	7.63

uncertainty of approximately ±3.1 per cent, for $3d^6(^5D)4s\ ^6D_{5/2} - 3d^7\ ^4F_{9/2}$ (3–6) this is ±5.5 per cent, and finally for $3d^6(^5D)4s\ ^6D_{9/2} - 3d^6(^5D)4p\ ^6D^o_{9/2}$ (1–16) is ±8.3 per cent. The uncertainty of the mean at each temperature for these transitions is given in Table 2.

While these uncertainties are useful for individual transitions at each temperature, the work of Fernández-Menchero, Zatsarinny & Bartschat (2017) for N IV has demonstrated that we cannot assign a reliable single valued uncertainty to the collisional data set as a whole. However, an uncertainty prescribed to a subset of DARC716 which encompasses transitions of astrophysical interest may be more appropriate for modelling applications. For such an analysis we use transitions between and within the first 25 even levels and first 25 odd levels over 22 temperature points ranging from 10^3 to 10^5 K, giving over 25 000 individual uncertainty measurements. Averaging over all temperatures and transitions considered, we assign an uncertainty of ±15 per cent to this 50 level subset of DARC716, which contains the low-lying forbidden and low-lying dipole transitions necessary to adequately model observation.

3 CLOUDY MODELLING

Given the earlier discussions of our data sets, we now choose to incorporate both the DARC262 and DARC716 data sets into the CLOUDY modelling code of Ferland et al. (2017). Our aim is not to use CLOUDY to undertake a detailed analysis of specific objects, but rather simply to produce sample synthetic Fe II spectra appropriate to typical AGN, to illustrate the usefulness of our atomic data. We compare these theoretical spectra with those generated using the Fe II data set that is in the current (2017) release of CLOUDY. This data set, which we denote C371, contains 371 levels ranging in energy up to 11.6 eV, and 68 635 transitions. The atomic data for Fe II in C371 includes a combination of data from experimental measurements, previous calculations, and $\bar{g}$ approximations (see Verner et al. 1999 and references therein).

In our CLOUDY models we employ the incident AGN continuum described by Korista et al. (1997),

$$f_v = v^{-0.5} \exp(-hv/kT_{BB}) \exp(-kT_{IR}/hv) + av^{-1}, \quad (2)$$

where T_{BB} and T_{IR} are the UV-Bump and infrared cut-off temperatures, respectively, and a is a parameter adjusted so that the correct UV to X-ray ratio α_{ox}, defined as

$$\frac{f_v(2keV)}{f_v(2500\text{Å})} = 403.3^{\alpha_{ox}}, \quad (3)$$

is obtained. We use solar abundances along with a hydrogen column density of 10^{24} cm^{-2}, a hydrogen-ionizing photon flux of $\log(\Phi_H) = 20$ cm^{-2} s^{-1}, a hydrogen density of $n_H = 10^9$ cm^{-3}, with $\alpha_{ox} = -1.4$ and $kT_{BB} = 44$ eV.

In Fig. 9 we present synthetic Fe II spectra across a portion of the UV and visible spectral regions from 100 to 500 nm. Reasonable agreement is found among all three data sets at wavelengths greater than about 200 nm, with some line peaks absent in the DARC262 plot due to missing transitions. Comparisons between DARC716 and C371 show better agreement, but with discrepancies in peaks and DARC716 providing additional lines around 300 nm. It is evident that the synthetic spectrum obtained from using the DARC262 data set is very sparse across the lower UV region from 100 to 150 nm. This wavelength range only contains 1018 lines, with approximately 6 per cent of these having radiative rates larger than 10^5 s^{-1}. Such few lines from DARC262 (and from existing models of comparable size) will obviously significantly limit the modelling of objects which show prominent Fe II emission features in the UV spectral region. Similarly, employing the existing C371 data set, we have a total of 4167 lines across the same 100 to 150 nm range. However, with DARC716 we have a total of 23791 lines across the same 50 nm interval, with more than 20 per cent of these having radiative transition rates larger than 10^5 s^{-1}. Of these, 308 are particularly strong, having radiative transition rates larger than 10^8 s^{-1}. In the future, we plan to undertake more detailed CLOUDY simulations of Fe II spectra using our new DARC716 data set, and assess and quantify its implication for the analysis of astronomical sources.

4 CONCLUSIONS

In this work we have investigated the electron-impact excitation of the iron-peak species Fe II. Discrepancies among existing effective collision strengths from earlier calculations in the literature have been highlighted, and addressed using three large-scale R-matrix scattering models, the target descriptions of which are sufficiently extensive enough to reach energies required for modelling astrophysical sources displaying strong UV emission and/or absorption lines of Fe II. The calculations presented provide the most extensive set of high quality atomic data currently available for Fe II, and will be useful for future astrophysical modelling applications.

An accurate representation of the Fe II atomic structure was calculated using GRASP^0 with 20 configurations giving 6069 fine-structure levels, and detailed comparisons with experimental measurements reveal good agreement. This model was carried through to substantial Dirac R-matrix calculations retaining 262 and 716 levels of the target structure in the close-coupling expansions. Another substantial Breit–Pauli R-matrix calculation was also presented, retaining the first 716 levels of a smaller six configuration CIV3 target structure. Convergence has been demonstrated for the energy mesh sizes, partial wave expansions, and close-coupling expansions

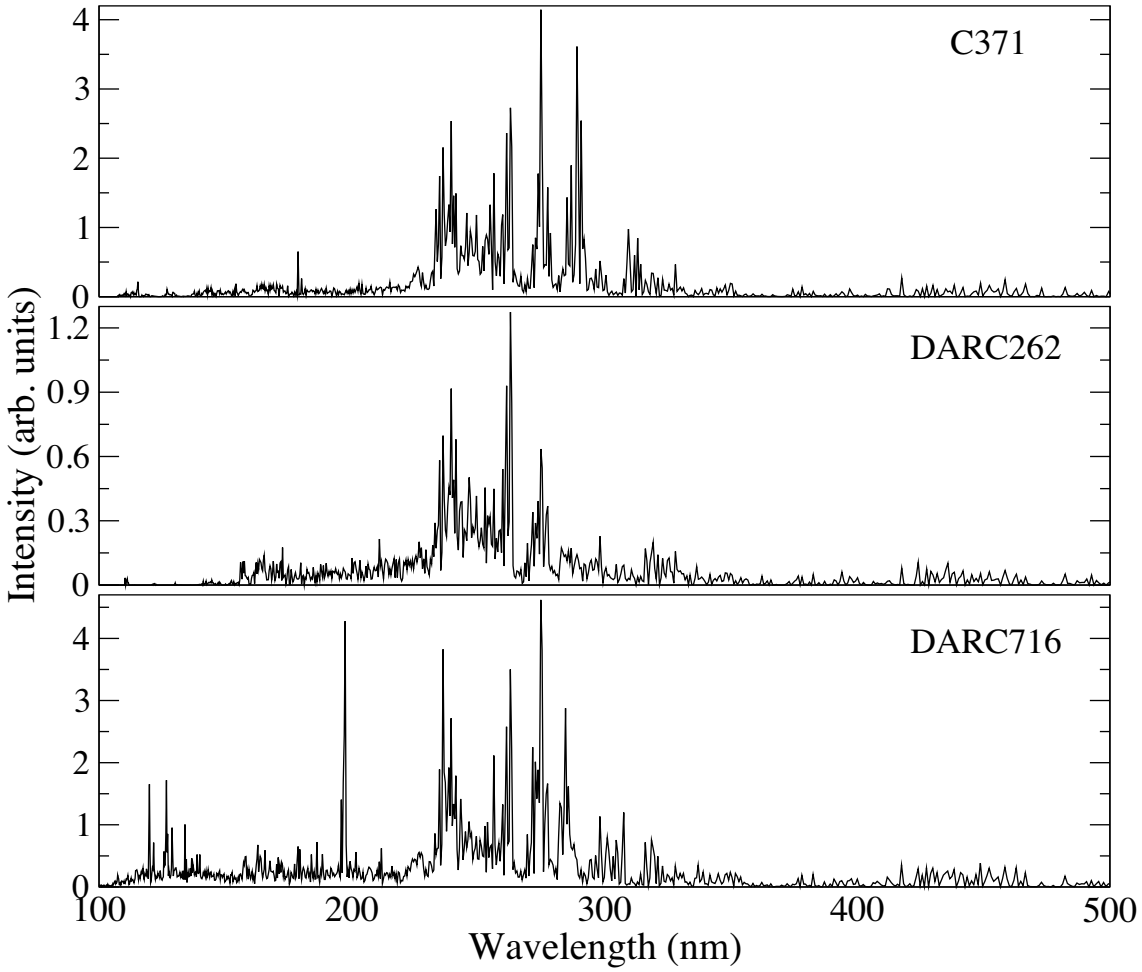

Figure 9. Synthetic Fe II spectra, calculated with the CLOUDY code, appropriate to AGN conditions. Top panel is the model calculated using the existing 371 level data set of Verner et al. (1999); middle panel is that using the DARC262 data set; and the bottom panel is that using the DARC716 data set.

employed, giving confidence in the reliability and accuracy of the scattering calculations. We have also demonstrated that in order to achieve convergence for the allowed transitions, a larger number of levels needs to be included in the close-coupling expansion to account for additional mixing with highly excited levels of the $3d^6 4p$, $3d^5 4s4p$ and $3d^6 5p$ configurations.

Collision strengths and effective collision strengths for low-lying forbidden and dipole transitions are presented and compared with available results in the literature. Very good agreement is found between the present 262 and 716 level DARC and 716 level Breit–Pauli calculations, and with the results of an existing 262 level Breit–Pauli calculation, but significant discrepancies are seen with results from smaller, less sophisticated calculations for the low-lying transitions. An analysis of the uncertainties in our calculations is presented, providing us with error bars on our effective collision strengths. Furthermore, by considering a 50 level subset of our DARC716 atomic data we are able to assign an uncertainty of ± 15 per cent to those astrophysically relevant forbidden and allowed transitions encompassed within that subset.

This new 716 level Dirac R-matrix data set was then incorporated into CLOUDY models to produce synthetic Fe II spectra applicable to typical AGN. Comparisons with spectra obtained using the existing atomic data within CLOUDY and the present 262 level Dirac R-matrix dataset reveals significantly more lines in portions of the UV region, highlighting the usefulness of this work for future modelling applications.

ACKNOWLEDGEMENTS

This work is supported by the UK Research and Innovation - Science and Technology Facilities Council grant award ST/P000312/1. All calculations were carried out on the Cray XC40 (Hazel Hen) supercomputer at the High Performance Computing Centre in Stuttgart and on a local computer cluster at Queen's University Belfast.

REFERENCES

Baluja K. L., Hibbert A., Mohan M., 1986, J. Phys. B: At. Mol. Phys., 19, 3613
Bautista M. A., Pradhan A. K., 1996, A&AS, 115, 551
Bautista M. A., Pradhan A. K., 1998, ApJ, 492, 650
Bautista M. A., Fivet V., Ballance C., Quinet P., Ferland G., Mendoza C., Kallman T. R., 2015, ApJ, 808, 174
Berrington K. A., Burke P. G., Hibbert A., Mohan M., Baluja K. L., 1988, J. Phys. B: At., Mol. Opt. Phys., 21, 339
Burgess A., 1974, J. Phys. B., 7, L364
Burke P., 2011, R-Matrix Theory of Atomic Collisions . Springer-Verlag, Berlin

Carpenter K. G., Ayres T. R., Harper G. M., Kober G., Nielsen K. E., Wahlgren G. M., 2014, ApJ, 794, 41
Clementi E., Roetti C., 1974, At. Data Nucl. Data Tables, 14, 177
Dyall K. G., Grant I. P., Johnson C. T., Parpia F. A., Plummer E. P., 1989, Comput. Phys. Commun., 55, 425
Eriksson M., Johansson S., Wahlgren G. M., 2006, A&A, 451, 157
Ferland G. J. et al., 2017, Rev. Mex. Astron. Astrofis., 53, 385
Fernández-Menchero L., Del Zanna G., Badnell N. R., 2015, MNRAS, 450, 4174
Fernández-Menchero L., Zatsarinny O., Bartschat K., 2017, J. Phys. B: At. Mol. Opt. Phys., 50, 065203
Hibbert A., 1975, Comput. Phys. Commun., 9, 141
Keenan F. P., Hibbert A., Burke P. G., Berrington K. A., 1988, ApJ, 332, 539
Korista K., Baldwin J., Ferland G., Verner D., 1997, ApJS, 108, 401
Leighly K. M., Halpern J. P., Jenkins E. B., Casebeer D., 2007, ApJS, 173, 1
NIST ASD Team, 2018, NIST *Atomic Spectra Database* (ver. 5.6.1). National Institute of Standards and Technology. Gaithersburg, Available at: https://physics.nist.gov/asd
Nussbaumer H., Storey P. J., 1980, A&A, 89, 308
Nussbaumer H., Pettini M., Storey P. J., 1981, A&A, 102, 351
Parpia F. A., Grant I. P., 1991, J. Physique, 01, C1
Pradhan A. K., Berrington K. A., 1993, J. Phys. B: At. Mol. Opt. Phys., 26, 157
Ramsbottom C., 2009, At. Data Nucl. Data Tables, 95, 910
Ramsbottom C. A. et al., 2002, J. Phys. B: At. Mol. Opt. Phys., 35, 3451
Ramsbottom C. A., Noble C. J., Burke V. M., Scott M. P., Burke P. G., 2004, J. Phys. B: At. Mol. Opt. Phys., 37, 3609
Ramsbottom C. A., Noble C. J., Burke V. M., Scott M. P., Kisielius R., Burke P. G., 2005, J. Phys. B: At. Mol. Opt. Phys., 38, 2999
Ramsbottom C. A., Hudson C. E., Norrington P. H., Scott M. P., 2007, A&A, 475, 765
Smith N., Hartigan P., 2006, ApJ, 638, 1045
Tayal S. S., Zatsarinny O., 2018, Phys. Rev., 98, 012706
Verner E. M., Verner D. A., Korista K. T., Ferguson J. W., Hamann F., Ferland G. J., 1999, ApJS, 120, 101
Zhang H. L., Pradhan A. K., 1995, A&A, 293, 953

This paper has been typeset from a TEX/LATEX file prepared by the author.